Influence of the Moiré Pattern of Ag(111)-Supported Graphitic ZnO on Water Distribution

Ting-Chieh Hung,^{1,*} Duy Le,² Talat Rahman,² and Karina Morgenstern¹

¹Lehrstuhl für Physikalische Chemie I, Ruhr-Universität Bochum,

Universitätstraße 150, Bochum D-44801, Germany

²Department of Physics, University of Central Florida, Orlando, FL 32816, USA

(Dated: June 20, 2022)

Abstract

The distribution of water on metal supported oxides is an important step in understanding heterogeneous catalysis such as in the water gas shift reaction. Here, we study water structures on Ag(111)-supported graphitic zinc oxide islands by variable temperature scanning tunneling microscopy around 150 K and *ab initio* calculations. Water clusters, accumulating on the ZnO islands, are confined to the hcp regions of the ZnO moiré pattern. A significantly higher cluster density at the island border is related to the dimensions of its capture zone. This suggests an upward mass transport of the water from the supporting metal to the ultrathin oxide film, increasing the water density at the active metal—oxide border.

Keywords: water clusters, ZnO, moiré pattern, metal-oxide border, STM, DFT

^{*} Ting-Chieh.Hung@rub.de

1. INTRODUCTION

The interaction of water with surfaces is important in several scientific and industrial applications. Despite the importance of ultrathin oxide films for heterogeneous catalysis, very little is known about water growth and distribution on them. It is known that water forms a 1D chain structure along the CaO<110> directions of a 20 ML CaO(001) film [1]. For iron oxide (FeO) on Pt(111), water clusters form on hydroxylated and non-hydroxylated ultrathin films [2]. In contrast to ultrathin FeO films, ultrathin films of ZnO supported on Ag(111) do not hydroxylate, not even upon exposure to molecular hydrogen or water [3]. Ultrathin film of 1 ML to 2 ML are graphitic on Au(111) [4] and Ag(111) [5] in contrast to thicker films [6] and thus different from bulk ZnO [7, 8]. On both surfaces, the bilayers stay almost flat, despite the different adsorptions sites of the bilayer ions [9]. Water molecules were calculated to adsorb on the Au(111)-supported graphitic ZnO bilayers forming two ordered superstructures at monolayer coverage after adsorption at 100 K and annealing to 200 K, (3×3) and $(\sqrt{3}\times\sqrt{3})R30^{\circ}$ at higher and lower coverage, respectively, superstructures that do not exist on any of the bulk ZnO single crystal surfaces [10]. Despite its importance for the water gas shift reaction, in particular at the catalytically active border between the oxide and the metal support, the initial water structures during growth on an ultrathin film of ZnO and its border have not yet been addressed in real space.

Much more explored are the water structure and growth on metal surfaces [11]. Water coverages in the submonolayer regime lead to structures up to 4 ML in height on various hydrophobic coinage metal surfaces, such as Cu(111) [12], Au(111) [13, 14], Ag(111) [15–17], and Ag(100) [18]. It suggests mass transport to higher layers during growth. For very low coverages, the most stable structure is a cyclic hexamer [19], which exists on Au(111) [14], Ag(111) [20], Cu(111) [19, 21], and on ultrathin FeO films on Pt(111) [2]. While on the coinage metals, clusters larger than nine molecules are polymorphous (e.g., [12, 17]), clusters up to 22 molecules have a distinct structures on iron oxide [2].

In this article, we investigate the growth of water clusters on graphitic ultrathin ZnO islands on Ag(111) by scanning tunneling microscopy (STM) at (150 ± 10) K and density functional theory (DFT) calculations. At submonolayer coverages, the water accumulates on the graphitic ZnO islands, forming clusters on the hcp regions of the moiré pattern with diameters between those of a water hexamer and the periodicity of the moiré pattern

(\sim 2.3 nm). The size of the capture zone of the ZnO islands highly influences the density of water clusters at their border. We discuss how the growth of the water is influenced by the zinc oxide moiré pattern, comparing the structure of the water clusters with that on Ag(111) and supported iron oxide.

2. METHODS

The STM measurements were performed in an ultrahigh vacuum (UHV) chamber with a base pressure better than 4×10^{-10} mbar. The UHV system consists of a separate deposition chamber, which is equipped with evaporators, and a combined preparation and measurement chamber, which combines the necessary equipment for sputtering and annealing with a commercial single-tube scanner STM (SPECS, "STM 150 Aarhus"). The sample is transferred between the preparation stages and the STM by a transfer rod. The STM is operated at a fast scanning speed (1 to 4 images/min) in the temperature range between 105 K and 350 K. The maximum scan range is (1500×1500) nm².

The Ag(111) surface was cleaned by repeated cycles of Ar⁺ ion sputtering at 1.3 keV $(p_{Ar} = 3 \times 10^{-5} \text{ mbar}, I_{sputter} = 3 \mu\text{A} \text{ to } 6 \mu\text{A}, t = 10 \text{ min to } 60 \text{ min})$ at room temperature (RT) followed by annealing the sample at 850 K to 900 K via electron bombardment $(I_{emi} = 16 \text{ mA}, V_{acc} = 1 \text{ kV}, t = 10 \text{ min to } 60 \text{ min})$ with the last cycle being shorter (5 min sputtering and 5 min annealing). The cleanliness of the Ag(111) was checked by STM.

The growth of the ZnO on the Ag(111) surface was carried out following an established procedure [4, 5, 22]. Zn was deposited at room temperature in an oxygen atmosphere ($p_{O_2} \sim 5 \times 10^{-6}$ mbar) followed by annealing at ~ 600 K for 10 min in UHV ($p \sim 5 \times 10^{-9}$ mbar). The metal was deposited via an electron-beam assisted evaporator (*Omicron*, EFM-3) from a Zn rod (*Goodfellow*, 2.0 mm in diameter, 99.99%). The evaporation material was outgassed under UHV conditions until the pressure stayed below 5.0×10^{-9} mbar. The coverage of the ZnO was determined by STM and is specified in percentages of the covered surface area. In this work, the ZnO covered between 15% and 75% of the Ag surface.

The D_2O (Sigma-Aldrich, isotopic purity of 99.9%) was filled into a glass tube that is connected to the UHV chamber via a leak valve. The D_2O was further purified in vacuum through several freeze-pump-thaw cycles. For the deposition, the leak valve was opened to

reach the desired pressure of $\sim 1 \times 10^{-7}$ mbar in the deposition chamber. During deposition, the sample was kept at a temperature around (130 \pm 5) K. The local coverages of D₂O were determined by STM and are given in percentage of the locally covered surface area (ZnO plus Ag). The D₂O occupation at the ZnO island border is given in percentage of the number of water-covered hcp regions parallel to this border.

We performed calculations using density functional theory (DFT) as implemented in the Vienna ab initio Simulation Package (VASP) [23] employing the projector-augmented wave (PAW) [24, 25] and the plane-wave basis set. We used the generalized-gradient approximation (GGA) in the form of the Perdew-Burke-Ernzerhof (PBE) [26, 27] functional together with DFT-D3 correction [28] to describe the electronic exchange-correlation. We set the electron kinetic energy cut-off for plane-wave expansion to 500 eV. To mimic the experimental observed structures of the moiré periodicity of graphitic ZnO on Ag(111), which is (7×7) - $ZnO/(8 \times 8)$ – Ag(111), we constructed a model supercell with a 5 layer (8 × 8) Ag(111) slab on one side of which we placed a (7×7) monolayer of graphitic ZnO at a starting distance of about 250 pm and a vacuum of about 1500 pm that separated the periodic image of the model system along the direction normal to the surface. The monolayer is representative for the graphitic ZnO(0001) structure that grows in this form up to 2 ML [6]. It is a suitable model system for the bilayer, investigated experimentally, at a reasonable computational cost. We used dipole corrections [29, 30] along the direction of the surface normal to cancel the effects of an artificial uniform electric field created by the asymmetric model system. All atoms, except for those in the bottom two Ag layers, were relaxed until all components of forces acting on each atom were less than 0.1 eV/nm. We sampled the Brillouin zone at the zone center and used Gaussian smearing with $\sigma = 0.1$ eV for structural relaxation. All electronic cycles were converged to 10^{-2} meV. The binding energy of H₂O on the model surface was evaluated using $E_b = (E_{sys} - E_{surf} - nE_{H_2O})/n$, where E_{sys} , E_{surf} , and E_{H_2O} are the total energies of the considered system, the surface, and the H₂O in isolated form (which is evaluated in an $1.5 \times 1.5 \times 1.5 \text{ nm}^3$ box), respectively, and n is the number of molecules in a supercell. Simulated STM images were approximated to be the iso-surface (10^{-3} e/nm^3) of the local density-of-states (LDOS) of all occupied states between the Fermi level and the simulated bias. The resulting images were convoluted with a Gaussian filter with a standard deviation of 0.1 nm to mimic the effect of the finite size of the STM tip.

3. RESULTS AND DISCUSSION

Before discussing the formation of D_2O structures in detail, we recapitulate the structure of ultrathin ZnO layers on Ag(111) [5, 22]. At a thickness of a bilayer, such layers are graphitic forming a moiré pattern due to their lattice mismatch with Ag(111) (inset

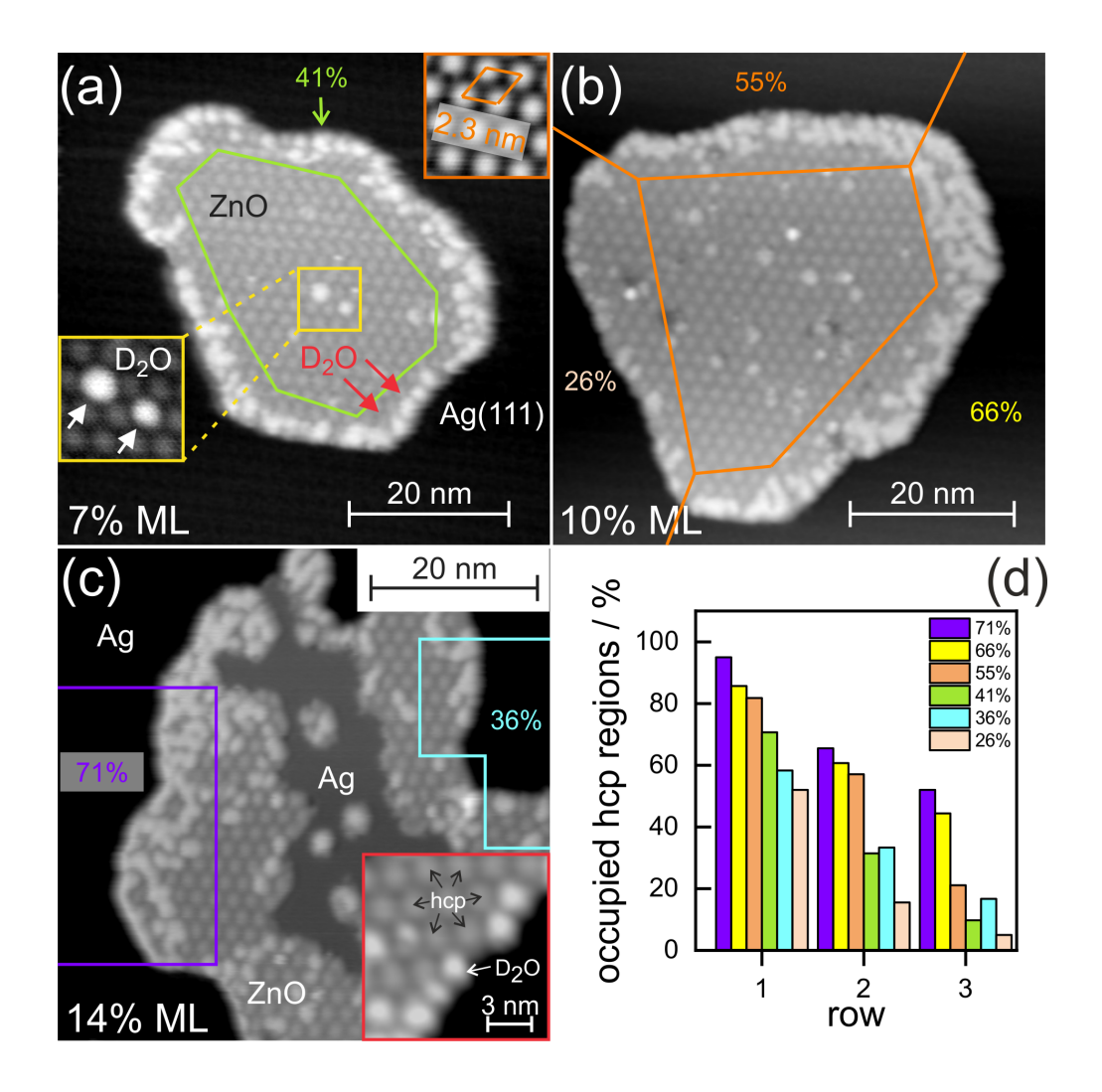


FIG. 1. Coverage dependence of D_2O on ZnO islands: (a to c) STM images at local coverages of (a) 7% ML, (b) 10% ML, and (c) 14% ML; inset in panel (a): pristine ZnO, region in yellow frame enlarged by a factor of 2 in panel (a); inset in panel (c): high-resolution STM image for D_2O clusters near the ZnO border. (d) Percentage of hcp regions on ZnO moiré pattern occupied by D_2O clusters for different parts of the border of the island as labeled in panels (a), (b), and (c). The STM images were all recorded at 1.5 V and (a) $I_t = 180$ pA, (140 ± 1) K, (b) $I_t = 140$ pA, (143 ± 1) K, and (c) $I_t = 130$ pA, (159 ± 1) K, inset: $I_t = 120$ pA, (148 ± 1) K.

in Fig. 1a). The unit cell length of this moiré pattern is ~ 2.3 nm, determined here as a $\rm ZnO(0001)$ – $(7 \times 7)/\rm Ag(111)$ – (8×8) coincidence structure. As the ZnO bilayer on the Ag(111) was calculated to be atomically flat without rumpling, [9], the moiré pattern is not of geometric but of electronic origin. The protrusions of the ZnO moiré pattern are assigned to the regions called hcp regions [4], which have one Zn atom adsorbed near an hcp site of Ag(111) framed by three O atoms adsorbed near atop sites, based on simulated STM images (see supporting information, Fig. S1). Our results are in good agreement with those obtained for the ZnO bilayer supported by Au(111) [4], a surface that has the same lattice constant as Ag(111). Concerning its interaction with water, we recall that the ultrathin film of ZnO supported by Ag(111) does not hydroxylate, not even upon adsorption of molecular hydrogen or water [3]. Furthermore, water molecules deposited on such an ultrathin ZnO film do not dissociate at the deposition and scanning temperatures between 130 K and 160 K used here [31].

D₂O at a local coverage between 7% ML to 14% ML forms clusters on the ZnO islands of the partially covered ZnO/Ag(111) surface (Fig. 1a to Fig. 1c). Two different cluster densities exist in Fig. 1a. At the interior of the ZnO islands, there is a low density of clusters (white arrows in yellow-bordered magnification in Fig. 1a). The border of the ZnO island is much more densely populated; the D₂O forms a rim of clusters along the island border (red arrows in Fig. 1a). In both parts, the D₂O clusters are exclusively nucleated at the protrusions of the ZnO moiré pattern, i.e., its hcp regions (inset in Fig. 1c). This preference is confirmed by our DFT calculations (see below). At increasing local D₂O coverage, more clusters nucleate while their size hardly changes (Fig. 1b and Fig. 1c). Only a few additional clusters nucleate in the interior of the islands, while the cluster density at their borders increases more substantially, filling the second and third row of the moiré pattern from the island borders. This observation is quantified in a histogram of the percentage of the occupied hcp regions by D₂O clusters for the first three rows from the island borders (Fig. 1d). Also along these, the D₂O coverage is not homogeneous. In order to compensate for the different local coverages, we separate the islands into parts with different hcp region occupations of the three rows from the island borders. We compare the three rows closest to the island borders for six hcp region occupations (Fig. 1d). In general, the individual occupation in every row increases with local hcp region occupation. The first row is occupied by around 60% for an hcp region occupation below 36% and more than 80% above 55% hcp region occupation. The second row is occupied by 16% at the lowest occupation of $\sim 26\%$. The occupation doubles and triples for hcp region occupations of around 40% and above 55%, respectively. This trend continues for the third row, in which less than 20% of the hcp regions are occupied by D_2O clusters at an occupation below 55%. This points to an inward mass transport of water accumulated at the border to more interior parts of the islands with increasing local water coverage.

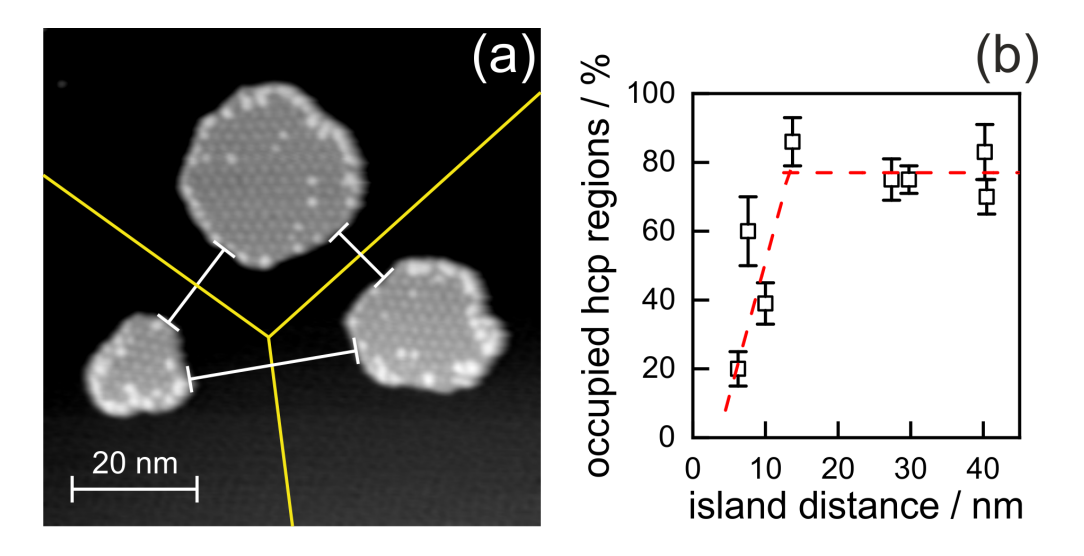


FIG. 2. Distribution of D_2O accumulated at the borders of ZnO islands: (a) STM image at 4% ML local coverage of D_2O deposited at (130 ± 5) K, scanning parameters: $V_t = 1.5$ V, $I_t = 90$ pA, (144 ± 1) K. Yellow lines: borders of the capture zone, white lines: nearest distances between ZnO islands (b) relationship between the percentage of D_2O clusters occupying the hcp regions and the nearest distances between ZnO islands; squares: experimental data; red dashed lines: two linear regressions for increasing and saturation range.

To understand the highly inhomogeneous distribution along the island border, we point out that there are no D_2O clusters on the bare part of the Ag(111) surface at any of the examined D_2O coverages. We further recall that the temperature during deposition of ~ 130 K is below the desorption temperature of water from Ag(111) [32] but that the water molecules are highly mobile at this temperature [16]. We thus propose that the high density of water at the border originates from the water molecules adsorbed on the bare Ag(111) but nucleated at the border of the ZnO islands. For this scenario, the occupation of the hcp regions should depend on the capture zone around the ZnO islands. This proposition is verified for ZnO islands in close proximity. At a low local D_2O coverage of 4% ML, the

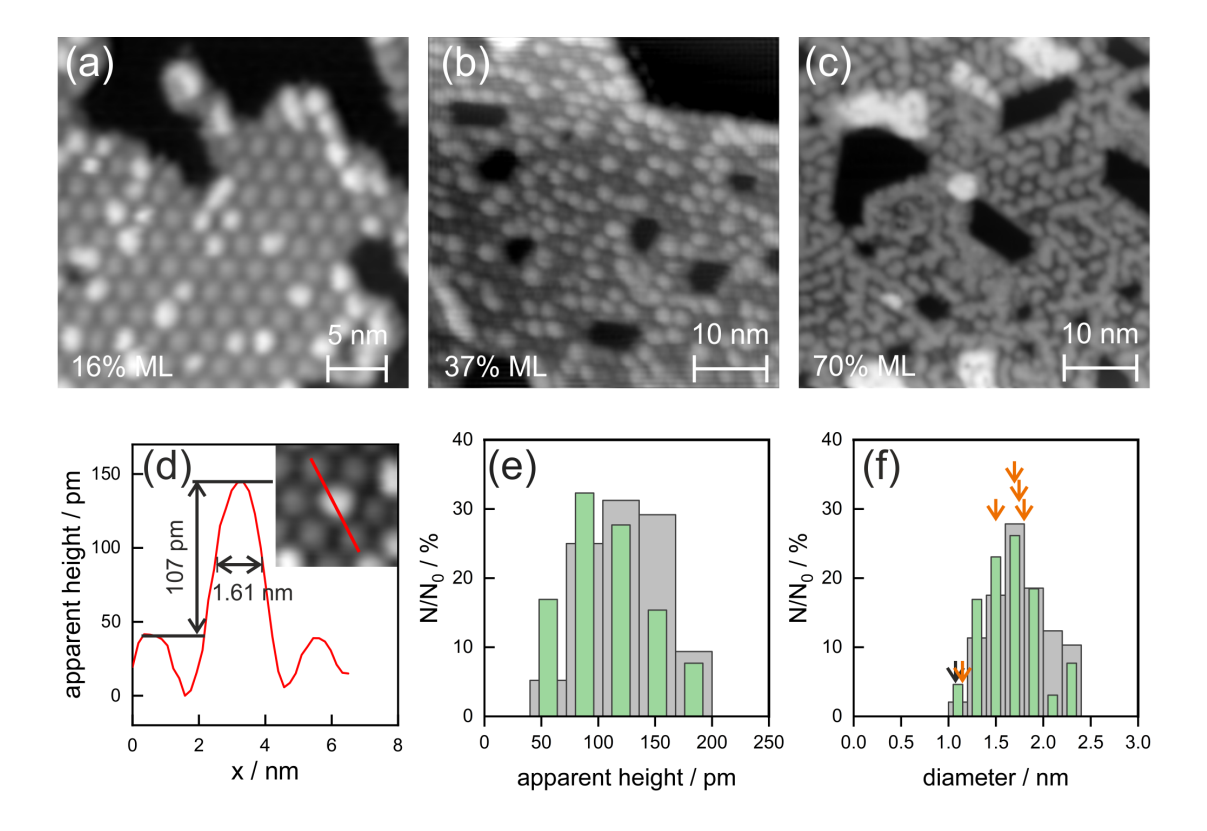


FIG. 3. Coverage-dependent geometry of D₂O clusters on ZnO layers: (a to c) STM images for D₂O coverages of (a) 16% ML, (b) 37% ML, and (c) 70% ML (d) Height profile of a typical D₂O cluster at a local coverage of 16% ML on a ZnO hcp region along red line as marked in inset (e) apparent height and (f) diameter distribution for two coverages of 16% ML (green, N₀ = 65) and 37% ML (gray, N₀ = 98). Black arrow in (f) marks the smallest D₂O clusters found on the ZnO moiré pattern; orange arrows mark the longest axes of water clusters on the ultrathin film of hydroxylated FeO (estimated from Fig. 3b in [2]). Scanning parameters: (a) $V_t = 1.5$ V, $I_t = 130$ pA, (159 ± 1) K, (b) $V_t = 1.5$ V, $I_t = 120$ pA, (143 ± 1) K, and (c) $V_t = 1.3$ V, $I_t = 330$ pA, (142 ± 1) K.

first row of three ZnO islands is only partly covered by D₂O (Fig. 2a). Indeed, there are fewer D₂O clusters at the border of the ZnO islands facing other ZnO islands than at the other borders. To quantify this observation, we relate the occupation of the hcp regions at the borders of the islands to the nearest distance between two ZnO islands. Normalization to the size of the capture zone, i.e., the distances between ZnO islands, compensates for the influence of different ZnO coverages. The capture zone is approximated by constructing a Voronoi diagram [33] based on the center positions of the ZnO islands (Fig. 2a). In the

capture zone, we measure the cluster density at that part of the border belonging to this zone. At increasing distance between two ZnO islands, the cluster density at the ZnO border increases from $\sim 20\%$ at ~ 7 nm distance to above $\sim 80\%$ at ~ 12 nm distance, above which it saturates (Fig. 2b). This dependence confirms that the high occupation of the hcp regions of ZnO by the water clusters at the ZnO island borders results from water molecules that were adsorbed on Ag(111), then diffused to a border of an island and onto it, and finally nucleated on hcp regions of the moiré pattern. At an increasing occupation of the hcp regions closest to the island borders, the molecules diffused on the islands to nucleate at more interior hcp regions.

Having understood the highly inhomogeneous distribution of the water clusters on the ZnO islands, we now turn to investigate their structure. At the island borders (Fig. 2a), as well as the interior of the island (yellow frame in Fig. 1a) and on almost closed ZnO layers (Fig. 3a and Fig. 3b), the size of the D_2O clusters is rather small and uniform up to coverages of around 70% ML. Only at this coverage and above, the D_2O clusters connect across hep regions to form longer chains (Fig. 3c). The cluster growth is distinctly different from that on homogeneous surfaces such as Ag(111) at a similar temperature of (118 \pm 3) K [16]. On homogeneous surfaces, water clusters grow larger with increasing coverage at almost constant cluster density [15–17] while here the cluster density increases.

For a geometric analysis, we concentrate on clusters that occupy one hcp region only. We characterize the close to circular D_2O clusters geometrically as exemplified in Fig. 3d. The diameter is measured as its broadest full width at half maximum (FWHM). The apparent height refers to the hcp-related protrusions of the moiré pattern. At a bias voltage of 1.5 V, the apparent height histogram hardly changes, ranging from 43 pm to 200 pm at an average of (108 ± 17) pm for the local coverage of 16% ML and (126 ± 18) pm for a local coverage of 37% ML (Fig. 3e). As there are no apparent heights reported so far for water clusters on oxide surfaces, we compare these values to the apparent heights measured on the coinage metal surfaces. The apparent heights of the D_2O clusters on ZnO measured here at 1.5 V are mostly larger than those of small single-layer clusters on coinage metal surfaces such as Au(111) (\sim 90 pm) [14] and Cu(111) (\sim 85 pm) [34], measured at -100 mV and 20 mV, respectively. As the apparent heights of amorphous and crystalline ice on Cu(111) increase at 58 pm/V and 40 pm/V, respectively [12], the height is nonetheless consistent with single-layer clusters.

Likewise, the diameter of the D_2O clusters on ZnO depends only slightly on coverage, varying between 1.1 nm and 2.3 nm at an average of (1.63 ± 0.15) nm for the local coverage of 16% ML and (1.74 ± 0.16) nm for the local coverage of 37% ML (Fig. 3f). The range suggests

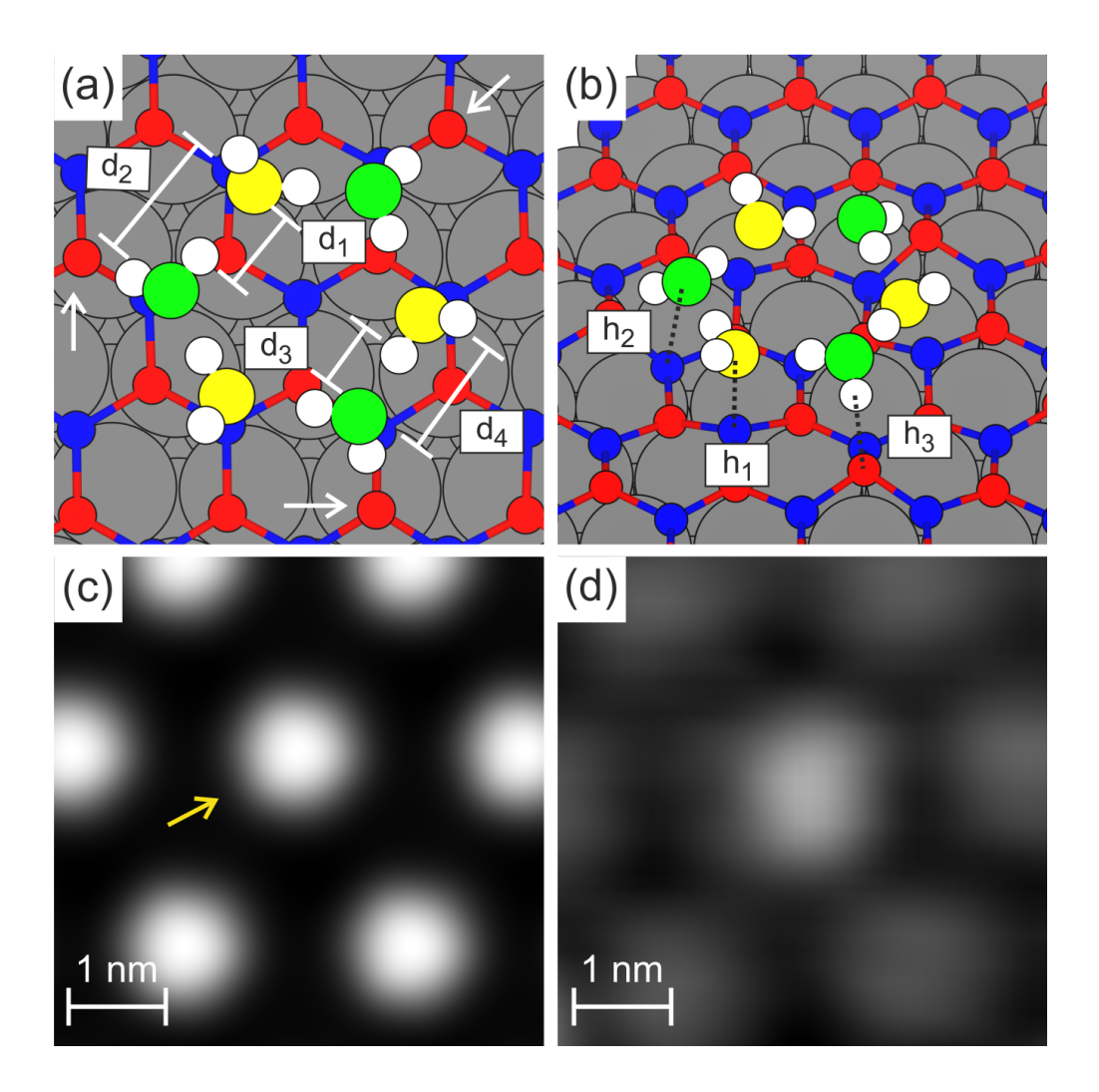


FIG. 4. Structure of water hexamer on hcp region: DFT-calculated structure in (a) top and (b) tilted view, color code: blue: Zn atoms, red: O atoms from ZnO, yellow: O atoms from water bound to Zn atoms, green: O atoms from hydrogen-bonded water, and white: H atoms. d_1 , d_3 , and h_3 are the hydrogen bond distances, d_2 and d_4 are the O-O distances between the water molecules, h_1 and h_2 are the heights of the water O atoms above the surface Zn atoms; white arrows point to the hydrogen-bonded surface O atoms (c) Gaussian-filtered simulated STM image of seven water hexamers on hcp regions of the ZnO moiré pattern at a tunneling voltage of 1.5 V; yellow arrow points out a water hexamer (d) STM image of the smallest D_2O cluster at the same scale and same voltage as (c), scanning parameters: $V_t = 1.5 \text{ V}$, $I_t = 130 \text{ pA}$, $(142 \pm 1) \text{ K}$.

that clusters of several sizes coexist, despite its being much narrower than on a homogeneous surface. The diameters are in the range of those measured with a molecular resolution for clusters of monolayer height on a related surface, the ultrathin FeO film (orange arrows in Fig. 3f). On both moiré patterned oxides, the clusters are distinctly different from islands grown on the homogeneous coinage metal surface [16, 18].

To understand the preference of water adsorption on the hcp regions, we carried out DFT calculations of a water hexamer adsorbed on the three regions, i.e., hcp, fcc, and atop, of the ZnO moiré pattern. The hexamer structure is similar to the stable structure for water hexamers on the low index coinage metals [14, 19–21] and ultrathin FeO film [2]. Our DFT calculation confirms that the water hexamer prefers to adsorb on the hcp region of the ZnO moiré pattern with binding energies per H₂O molecule of 0.735 eV, 0.705 eV, and 0.705 eV for the adsorption at hcp, atop, and fcc, respectively.

In the hexamer structure, three of the water molecules bind directly to the surface Zn atoms via their O atoms (yellow in Fig. 4a), referred herein to as surface-bonded H₂O. The other three water molecules (green in Fig. 4a) are hydrogen-bonded to the surface-bonded H₂O molecules with one additional OH group whose hydrogen binds to nearby surface O atoms (white arrows in Fig. 4a). The hydrogen-bonded water molecules (green in Fig. 4a and Fig. 4b) are rotated such that their dangling OH groups point toward a surface O atom. Their hydrogen bonding results in an outward relaxation of this O atom (marked by white arrows in Fig. 4a). Its bonding strength is reflected in the rather short hydrogen bond length of 191 pm (h₃ in Fig. 4b). The hydrogen bonding distances between the water molecules alternate between 196 pm (d_1 in Fig. 4a) and 160 pm (d_3 in Fig. 4a). It leads to the six non-equal O-O distances in the water hexamer, alternating between 294 pm (d₂ in Fig. 4a) and 263 pm (d₄ in Fig. 4a). Both distances are smaller than the Zn–Zn distance of 329 pm, such that the adsorption sites of the water molecules are slightly shifted from the atop site of the Zn atoms. Moreover, the water molecules in the hexamer are not adsorbed at the same height above the surface. Instead, the three surface-bonded water molecules are closer to the surface than the other three with O–Zn distances of 221 pm (h₁ in Fig. 4b) and 298 pm (h₂ in Fig. 4b), respectively. This buckling by 77 pm is, remarkably, the same as that of a water hexamer on a metal surface, Cu(111), of 76 pm [19].

Similar hexameric structures develop on both hydroxylated and non-hydroxylated regions of ultrathin FeO films [2]. On the non-hydroxylated FeO, while all water molecules of the

hexamer are hydrogen-bonded with each other, only half of them bind to the surface O atoms [2], as on ZnO. In contrast to the structure on ZnO, the surface-bonded water molecules bind via their OH groups to surface oxygen and not via their lone pairs to the metal. Moreover, the free OH of the hydrogen-bonded water molecules point outward for FeO, but form a weak hydrogen bond with a surface oxygen for ZnO. We relate these differences to the buckled structure of FeO, which suppresses binding to the iron. On the hydroxylated ultrathin FeO film, in addition to half of the water molecules in the hexamers forming OH groups to surface oxygen, the other half binds to the hydroxylated oxygen through their oxygen lone pair [2], stabilizing the hexamer.

The hexamer leads to a round protrusion in a simulated STM image with a diameter of \sim 1.0 nm (yellow arrow in Fig. 4c), very close to the smallest water cluster in experiments, at a diameter of ~ 1.1 nm (Fig. 4d). Both shapes are circular, thus confirming that the smallest D₂O cluster on the ZnO is a hexamer at the hcp region of ZnO (Fig. 4d). Only very few clusters exhibit this small size at the investigated coverages (black arrow in Fig. 3f). Larger water clusters on hydroxylated FeO thin films are formed by combining several water hexamers [2]. For the Ag(111)-supported ZnO bilayer, our DFT results reveal that two combined water hexamers are unstable because the distance between two oxygen atoms in the water hexamers is smaller than that between the Zn atoms in the ZnO layer. Though of similar size, the larger D₂O clusters on ZnO are thus structured differently than those on hydroxylated FeO thin film, presumably due to the stabilizing effect of the direct binding of all water molecules to the surface. Water adsorbed on the related Au(111)-supported ZnO bilayer forms two hexagonal- and zigzag-conformation $(\sqrt{3} \times \sqrt{3})R30^{\circ}$ at lower and a (3×3) superstructures at higher near monolayer coverage [10]. An extended hexamer structure would correspond to a $(\sqrt{3} \times \sqrt{3})R30^{\circ}$ superstructure, suggesting that the larger structures on the Ag(111)-supported ZnO bilayer here correspond to patches of the two calculated hexagonal- and zigzag-conformation water structures on the Au(111)-supported ZnO, confined to the hcp regions of moiré pattern.

We finally point out three major differences in water nucleation on ultrathin ZnO as compared to ultrathin FeO. First, the water clusters nucleate and grow exclusively at the hcp regions of the ultrathin ZnO film (Fig. 3a and Fig. 3b) up to a local water coverage of $\sim 70\%$ ML, while they form extended islands on the bare ultrathin FeO film already at low coverage. Only on the hydroxylated ultrathin film, small and separated water clusters are

confined to the fcc domains of the moiré pattern [2]. It implies that on the non-hydroxylated FeO ultrathin film, the energy difference between different regions is considerably smaller than on the ZnO ultrathin film.

Second, the water clusters nucleate on the fcc regions of the hydroxylated FeO moiré pattern [2], but on the hcp regions of the ZnO moiré pattern. On the hydroxylated domains of the FeO moiré pattern, the water structures are stabilized by three water molecules accepting hydrogen bonds from surface hydroxylated oxygen [2]. The FeO film is more hydroxylated at its fcc region than on other regions, explaining the preference of water to nucleate on these regions.

Third, the water hexamer on the ZnO ultrathin film is, at 77 pm, more buckled than that on the FeO ultrathin film with 10 pm to 25 pm, at least on the hydroxylated one, for which a value is stated in [2]. Both types of water molecules are differently bound to the two oxide surfaces. The ones binding through their lone pair (yellow in Fig. 4a) bind to the metal of the ZnO but to a hydroxyl of the FeO. The hydrogen bonds of the ones binding through the hydrogen bond is shorter on FeO than on ZnO, resulting in a stronger hydrogen bonding. A more similar bonding of all of the water molecules to the FeO than ZnO surface results in a flatter structure of the water hexamers, as compared to the situation discussed before.

4. CONCLUSION

We investigated the structure and distribution of water clusters on Ag(111)-supported graphitic ZnO islands with variable temperature scanning tunneling microscopy and ab initio calculations. We revealed multiple differences between the water clusters grown on hydroxylated and non-hydroxylated FeO ultrathin films and those on similar ZnO films. The ZnO moiré pattern confines the water clusters to its hcp regions. The highly-dispersed narrow-sized clusters present a favorable distribution of the water for further reactivity, e.g., in the water gas shift reaction. The pronounced higher cluster density at the border of the ZnO islands, regardless of the water coverage, suggests an upward mass transport of the water from the supporting metal to the oxide islands, increasing the water density at the catalytically active metal—oxide border. Our study on the structure and distribution of water clusters on ZnO assists future research on the first step of water adsorption in reactions including water as one of its reactants in heterogeneous catalysis.

5. SUPPORTING INFORMATION

Geometrical optimized structure of the ZnO supported by Ag(111) and corresponding simulated STM image.

6. ACKNOWLEDGMENTS

This work is funded by the Deutsche Forschungsgemeinschaft (DFG, German Research Foundation) under Germany's Excellence Strategy - EXC 2033 - 390677874 - RESOLV and the Research Training group "Confinement-controlled Chemistry", funded by the Deutsche Forschungsgemeinschaft (DFG) under Grant GRK2376/331085229. The work of DL and TSR (DFT calculations) is supported in part by NSF CHE1955343. Calculations were performed using the computing resources at the Advanced Research Computing Center at University of Central Florida and the National Energy Research Scientific Computing Center.

7. REFERENCES

- [1] Zhao, X.; Shao, X.; Fujimori, Y.; Bhattacharya, S.; Ghiringhelli, L. M.; Freund, H.-J.; Sterrer, M.; Nilius, N.; Levchenko, S. V. Formation of Water Chains on CaO(001): What Drives the 1D Growth? J. Phys. Chem. Lett. 2015, 6, 1204–1208.
- [2] Merte, L. R.; Bechstein, R.; Peng, G.; Rieboldt, F.; Farberow, C. A.; Zeuthen, H.; Knudsen, J.; Lægsgaard, E.; Wendt, S.; Mavrikakis, M.; Besenbacher, F. Water Clustering on Nanostructured Iron Oxide Films. *Nat. Commun.* 2014, 5, 4193–4200.
- [3] Liu, B.-H.; Boscoboinik, J. A.; Cui, Y.; Shaikhutdinov, S.; Freund, H.-J. Stabilization of Ultrathin Zinc Oxide Films on Metals: Reconstruction Versus Hydroxylation. J. Phys. Chem. C 2015, 119, 7842–7847.
- [4] Deng, X.; Yao, K.; Sun, K.; Li, W.-X.; Lee, J.; Matranga, Ch. Growth of Single- and Bilayer ZnO on Au(111) and Interaction With Copper. J. Phys. Chem. C 2013, 117, 11211–11218.

- [5] Shiotari, A.; Liu, B.-H.; Jaekel, S.; Grill, L.; Shaikhutdinov, S.; Freund, H.-J.; Wolf, M.; Kumagai, T. Local Characterization of Ultrathin ZnO Layers on Ag(111) by Scanning Tunneling Microscopy and Atomic Force Microscopy. J. Phys. Chem. C 2014, 118, 27428–27435.
- [6] Tusche, C.; Meyerheim, H. L.; Kirschner, J. Observation of Depolarized ZnO(0001) Monolayers: Formation of Unreconstructed Planar Sheets. Phys. Rev. Lett. 2007, 99, 026102-1– 206102-4.
- [7] Dulub, O.; Diebold, U.; Kresse, G. Novel Stabilization Mechanism on Polar Surfaces: ZnO(0001)-Zn. Phys. Rev. Lett. 2003, 90, 016102-1-016102-4.
- [8] Xu, H.; Dong, L.; Shi, X.; Liu, Y.; Hove, M. A. V.; Lin, N.; Tong, S. Y. Observation and Analysis of Ordered and Disordered Structures on the ZnO(0001) Polar Surface. J. Phys. Chem. C 2016, 120, 26915–26921.
- [9] Tosoni, S.; Li, C.; Schlexer, P.; Pacchioni, G. CO Adsorption on Graphite-Like ZnO Bilayers Supported on Cu(111), Ag(111), and Au(111) Surfaces. J. Phys. Chem. C 2017, 121, 27453– 27461.
- [10] Deng, X.; Sorescu, D. C.; Lee, J. D₂O Interaction with Planar ZnO(0001) Bilayer Spported on Au(111): Structures, Energetics and Influence of Hydroxyls. J. Phys. Chem. C 2016, 120, 8157–8166.
- [11] Hodgson, A.; Haq, S. Water Adsorption and the wetting of Metal Surfaces. Surf. Sci. Rep. 2009, 64, 381–451.
- [12] Mehlhorn, M.; Morgenstern, K. Height Analysis of Amorphous and Crystalline Ice Structures on Cu(111) in Scanning Tunneling Microscopy. New J. Phys. **2009**, 11, 093015–093028.
- [13] Gawronski, H., Morgenstern, K., Rieder, K.-H. Electronic Excitation of Ice Monomers on Au(111) by Scanning Tunneling Microscopy. Eur. Phys. D 2005, 35, 349-353.
- [14] Dong, A.; Yan, L.; Sun, L.; Yan, S.; Shan, X.; Guo, Y.; Meng, S.; Lu, X. Identifying Few-Molecule Water Clusters with High Precision on Au(111) Surface. ACS Nano 2018, 12, 6452–6457.
- [15] Heidorn, S.-C.; Bertram, C.; Morgenstern, K. The Fractal Dimension of Ice on the Nanoscale. Chem. Phys. Lett. 2016, 665, 1–5.
- [16] Heidorn, S.-C., Lucht, K.; Bertram, C.; Morgenstern, K. Preparation-Dependent Orientation of Crystalline Ice Islands on Ag(111). J. Phys. Chem. B 2018, 122, 479–484.

- [17] Heidorn, S.-C.; Bertram, C.; Morgenstern, K. Low-Temperature Growth of Amorphous Water Ice on Ag(111). J. Phys. Chem. C 2018, 122, 15304–15310.
- [18] Bakradze, G.; Morgenstern, K. Temperature-dependent Shape Change of Ice Nanoclusters on Ag(100). *ChemPhysChem* **2018**, *19*, 2858–2862.
- [19] Michaelides, A.; Morgenstern, K. Ice Nanoclusters at Hydrophobic Metal Surfaces. Nat. Mat. 2007, 6, 597–601.
- [20] Morgenstern, K.; Nieminen, J. Imaging Water on Ag(111): Field induced Reorientation and Contrast Inversion. J. Chem. Phys. 2004, 120, 10786–10791.
- [21] Duan, S.; Zhang, I. Y.; Xie, Z.; Xu, X. Identification of Water Hexamer on Cu(111) Surfaces. J. Am. Chem. Soc. 2020, 142, 6902–6906.
- [22] Pan, Q.; Liu, B.-H.; McBriarty, M. E.; Martynova, Y.; Groot, I. M. N.; Wang, S.; Bedzyk,
 M. J.; Shaikhutdinov, S.; Freund, H.-J. Reactivity of Ultra-Thin ZnO Films Supported by
 Ag(111) and Cu(111): A Comparison to ZnO/Pt(111). Catal. Lett. 2014, 144, 648-655.
- [23] Kresse, G.; Furthmüller, J. Efficiency of *Ab-Initio* Total Energy Calculations for Metals and Semiconductors Using a Plane-Wave Basis Set. *Comput. Mater. Sci.* **1996**, *6*, 15–50.
- [24] Blöchl, P. E. Projector Augmented-Wave Method. Phys. Rev. B 1994, 50, 17953–17979.
- [25] Kresse, G.; Joubert, D. From Ultrasoft Pseudopotentials to the Projector Augmented-Wave Method. Phys. Rev. B 1999, 59, 1758–1775.
- [26] Perdew, J. P.; Burke, K.; Ernzerhof, M. Generalized Gradient Approximation Made Simple. Phys. Rev. Lett. 1996, 77, 3865–3868.
- [27] Perdew, J. P.; Burke, K.; Ernzerhof, M. Erratum: Generalized Gradient Approximation Made Simple. *Phys. Rev. Lett.* **1997**, *78*, 1396–1396.
- [28] Grimme, S.; Antony, J.; Ehrlich, S.; Krieg, H. A Consistent and Accurate Ab-Initio Parametrization of Density Functional Dispersion Correction (DFT-D) for the 94 Elements H-Pu. J. Chem. Phys. 2010, 132, 154104-1-154104-19.
- [29] Bengtsson, L. Dipole Correction for Surface Supercell Calculations. Phys. Rev. B 1999, 59, 12301–12304.
- [30] Neugebauer, J.; Scheffler, M. Adsorbate-Substrate and Adsorbate-Adsorbate Interactions of Na and K Adlayers on Al(111). Phys. Rev. B 1992, 46, 16067–16080.
- [31] Yu, X.; Roth, J. P.; Wang, J.; Sauter, E.; Nefedov, A.; Heißler, S.; Pacchioni, G.; Wang, Y.; Wöll, Ch. Chemical Reactivity of Supported ZnO Clusters: Undercoordinated Zinc and

- Oxygen Atoms as Active Sites. ChemPhysChem 2020, 21, 2553–2564.
- [32] Carley, A. F.; Davies, P. R.; Roberts, M. W.; Thomas, K. K. Hydroxylation of Molecularly Adsorbed Water at Ag(111) and Cu(100) Surfaces by Dioxygen: Photoelectron and Vibrational Spectroscopic Studies. Surf. Sci. Lett. 1990, 238, L467–L472.
- [33] Voronoi, G. Nouvelles applications des paramètres continus à la théorie des formes quadratiques. Deuxième mémoire. Recherches sur les parallélloèdres primitifs. (New Applications of Continuous Parameters to the Theory of Quadratic Forms. Second Memory. Research on Primitive Parallelohedra.) J. Reine Angew. Math. 1908, 134, 198–287.
- [34] Morgenstern, K.; Rieder, K.-H. Formation of the Cyclic Ice Hexamer via Excitation of Vibrational Molecular Modes by the Scanning Tunneling Microscope. J. Chem. Phys. 2002, 116, 5746–5752.

8. TOC GRAPHIC